European Cells and Materials Vol. 46 2023 (pages 40-56) DOI: 10.22203/eCM.v046a03 ISSN 1473-2262

# RELATIONSHIP BETWEEN MICROSCALE SHEAR MODULUS, COMPOSITION, AND STRUCTURE IN PORCINE, CANINE, AND HUMAN TEMPOROMANDIBULAR-JOINT CARTILAGE: RELEVANCE TO DISEASE AND DEGENERATION

D. Yoon[1], S. Peralta[2], N. Fiani[2], G.S. Reeve[3], I. Cohen[4] and L.J. Bonassar[1,5,*]

[1] Sibley School of Mechanical and Aerospace Engineering, Cornell University, Ithaca, NY, USA
[2] Department of Clinical Sciences, College of Veterinary Medicine, Cornell University, Ithaca, NY, USA
[3] Oral and Maxillofacial Surgery, Weill Cornell Medicine, New York, NY, USA
[4] Department of Physics, Cornell University, Ithaca, NY, USA
[5] Meinig School of Biomedical Engineering, Cornell University, Ithaca, NY, USA

**Abstract**

Fully understanding the complex mechanical function of temporomandibular joint (TMJ) cartilage and the compositional and structural organization that underlie it is a persistent challenge. Changes to composition, structure, and mechanics take place in naturally occurring disease in humans and canines as well as in disease models, such as in pigs. This study combined histology, Fourier transform infrared (FTIR) microscopy, Fast Fourier transform (FFT), and confocal elastography to quantify the relationship between the microscale composition, structure, and shear mechanics of porcine, canine, and human TMJ cartilage. All three species had distinct zonal mechanics and similarly high stiffness of 105~106 Pa in the hypertrophic zone. Notably, porcine tissue had a thick, compliant fibrous zone (~ 200 μm) ($G^* < 104$ Pa) that was absent in canine and human tissue. The hypertrophic zone of all three species had high proteoglycan content, while the surface regions showed higher collagen content and fiber orientation. Small changes (two-fold) in composition led to large changes (twenty-fold) in modulus. Structural orientation of the fibers showed that high fiber orientation led to more compliant tissue mechanics while the angle of orientation was not predictive of the shear mechanics. The relationship between local composition, structure, and mechanics were similar in all three species. Despite this similarity, the immature pigs used most frequently in disease models have a very thick compliant surface region, the presence of which is likely to alter the degenerative process.

**Keywords**: Elastography, rigidity percolation, Fourier Transform Infrared microscopy, collagen, proteoglycan, extracellular matrix, Fast Fourier Transform image analysis.

***Address for correspondence**: Lawrence J. Bonassar PhD, Daljit S. and Elaine Sarkaria Professor, Meinig School of Biomedical Engineering, Sibley School of Mechanical and Aerospace Engineering, 149 Weill Hall, Cornell University, Ithaca, NY, 14853, USA
Telephone number: (607) 255-9381 Email: lb244@cornell.edu

**List of Abbreviations**

| | |
|---|---|
| TMJ | Temporomandibular joint |
| TMJD | Temporomandibular joint disorder |
| FTIR | Fourier transform infrared |
| TDIS | Tissue deformation imaging stage |
| FFT | Fast Fourier Transform |
| MCT | Mercury-Cadmium-Telluride |
| 5-DTAF | 5-dicholorotriazinyl-aminofluorscein |
| ROI | Region of interest |
| SM | Shear modulus |
| ECM | Extracellular matrix |
| OI | Orientation index |

## Introduction

The temporomandibular joint (TMJ), consisting of the mandibular condyle, the TMJ disc, and the fossa-eminence complex (Ingawalé and Goswami, 2009; Piette, 1993) is one of the most used joints in the human body (Alomar *et al*., 2007; American Association of Oral and Maxillofacial Surgeons, 2007). While TMJ disorders are highly prevalent and have been stated in early dental (Gysi, 1921; Tanaka and Koolstra, 2008) and medical (Costen, 1997; Tanaka and Koolstra, 2008) literature, the function of the joint is still poorly understood (Grant, 1973; Sharma *et al*., 2011; Wadwha and Kapila, 2008). With millions of people suffering from TMJ disorder (TMJD) in the United States alone (Wadhwa and Kapila, 2008), and with a large fraction of TMJD causes currently unexplained (Stegenga *et al*., 1992), the importance of understanding the complex function of this joint cannot be more emphasized.

In TMJD, it is not the usual case for bones to fail, but rather the softer tissues that form the articular surface (Sindelar and Herring, 2005). Alterations in the biomechanics of the TMJ may lead to the development or exacerbation of an existing condition (Singh and Detamore, 2009). The soft tissues, which include the mandibular condylar cartilage and the TMJ disc, play a crucial role in the underlying mechanics of the TMJ. Among the cartilaginous tissues of the TMJ, the TMJ disc has received the most attention, but much is unknown about the TMJ cartilage (Detamore and Athanasiou, 2003a; Detamore and Athanasiou, 2003b; Kim *et al*., 2003). This unique tissue is distinct from the articular hyaline cartilage in other joints (Milam, 2003; Singh and Detamore, 2009). As such, understanding how these distinct structural and compositional properties relate to the local mechanics of the TMJ cartilage is crucial.

Unlike other synovial joints, (Elhamian *et al*., 2015; Hinton and Carlson, 2005; Kuroda, 2009) TMJ cartilage has four distinct zonal regions; namely, the fibrous surface, the proliferative, mature, and the hypertrophic zones (Kuroda, 2009). The fibrous surface layer is composed of highly aligned Type I collagen and has collagen fiber bundles greater than 50 μm (Kuroda, 2009). The regions underlying the fibrous surface are similar to hyaline cartilage in other joints (Wadhwa and Kapila, 2008). These structural and compositional characteristics of each zone lead to specific mechanical characteristics, which still are poorly understood.

Recent work has shown that this zonal structure gives rise to zonal shear mechanics (Gologorsky, 2021). However, the origins of these zonal mechanics are unclear. Other recent studies have identified critical relations between the structure, composition, and mechanics in hyaline cartilage using a combination of confocal elastography and Fourier transform infrared (FTIR) microscopy (Boys *et al*., 2019; Buckley *et al*., 2008; Middendorf *et al*., 2020; Silverberg *et al*., 2014; Sloan *et al*., 2020; Wyse Jackson *et al*., 2022). However, these techniques have not been applied to study TMJ cartilage and quantifying these properties are important to understand disease and degeneration.

Several preclinical animal models such as mice, rabbit, sheep, and minipig, exist to study TMJD (Almarza *et al*., 2018; Labus *et al*., 2021). Notably, porcine models are the most widely used species due to their ease of surgical accessibility to the TMJ,

particularly in young animals (Kuboki *et al*., 1997; Kang *et al*., 2000; Lowe *et al*., 2018; Singh and Detamore, 2008; Singh and Detamore, 2009; Tanaka *et al*., 2006; Tanaka *et al*., 2008). In contrast, naturally occurring disease and degeneration occurs in both humans (Wadhwa and Kapila, 2008) and canines and is more common with age and older animals (Arzi *et al*., 2021; Hammond *et al*., 2012; Maas and Theyse, 2007; Macready *et al*., 2010). The extent to which the structure and mechanics of young porcine tissue used for disease and degeneration models match that of species with naturally occurring disease is not known.

To address this knowledge gap, the goals of this study were to: 1) investigate the zonal characteristics of the local shear mechanics in porcine, canine, and human TMJ cartilage; and 2) identify the quantitative relationship between tissue composition and structure to the local shear mechanics in porcine, canine, and human TMJ cartilage.

## Materials and Methods

### Sample preparation

TMJ condyles were extracted from approximately 6~8 months old pig heads obtained from a local butchery (Schrader Farms Meat Market, Romulus, NY, USA), approximately 1-year old canines (College of Veterinary Medicine, Cornell University, Ithaca, NY, USA), and human cadavers (Weill Cornell Medicine, New York, NY, USA) (IRB exempt). Full thickness osteochondral explants (4 mm diameter) from four anatomic locations (central, medial, lateral, posterior) were obtained from the porcine condyle while two anatomic locations (central medial, central lateral) were obtained from canine and human cadaver samples (Fig. 1**a**,**b**). A total of four, ten, and three osteochondral explants were obtained from porcine, canine, and human condyles respectively. Osteochondral explants were bisected in the posteroanterior direction into hemicylinders. Bisected osteochondral explants were immediately frozen after collection. The condyles were stored without any buffer to prevent crystallization of the cartilage. One half was used for mechanical testing within a week of tissue harvest using a previously established method (Bartell *et al*., 2018; Buckley *et al*., 2008; Buckley *et al*., 2010) using a custom-built Tissue Deformation Imaging Stage (TDIS) setup on an inverted Zeiss LSM 510 5 live confocal microscope (Carl Zeiss AG, Oberkochen, Germany) and the other half was used for histological staining and FTIR (Bruker, Billerica, MA, USA).

### Histology

Histological staining of all three species samples were done by the Clinical Pathology Core (Cornell College of Veterinary Medicine, Ithaca, NY, USA). The hemicylinder explants were fixed in neutral buffer formalin (Fisher Scientific, Hampton, NH, USA) for 24–48 hours, rinsed with 70 % ethanol (Fisher Scientific, Hampton, NH, USA), decalcified, and sectioned in 4 μm thickness for staining. Safranin-O (Fisher Scientific, Hampton, NH, USA) was used to observe relative proteoglycan content and Picrosirius red (Sigma Aldrich, St. Louis, MO, USA) was used to observe relative collagen content. These sections were then imaged under a light microscope (Nikon Eclipse TE2000-S, Microvideo Instruments, Avon, MA, USA) (Fig. 1**c**).

### FTIR microscopy

A previously established protocol for articular cartilage, (Silverberg *et al*., 2014) was used where 4 μm thick sections were placed on a 3 mm thick IR-transparent barium fluoride slides (32 mm diameter) (Spectral Systems, Hopewell Junction, NY, USA). Sections were deparaffinized in three successive xylene baths and rehydrated with 100 %, 95 %, and 70 % ethanol baths (Sloan *et al*., 2020). Sample images were taken with a Hyperion 3000 FTIR microscope (Bruker, Billerica, MA) using compressed air purge to rid excess water vapor. A brightfield overview image was obtained to determine the region of interest from the cartilage surface through the depth of the tissue until the subchondral bone. FTIR absorbance spectra was obtained in transmission mode with a resolution of 4 $cm^{-1}$ using an IR-compatible 15× objective (Sloan *et al*., 2020). Spectra at each point were averaged over 16 background-corrected scans between 600 and 4,000 $cm^{-1}$. Image acqusition was done with a single element Mercury-Cadmium-Telluride (MCT) detector in conjunction with a scanning microscope

stage. The step size and aperture size were both set to 50 μm resulting in a 50 μm × 50 μm window.

*FTIR microscopy data analysis*

The amide I, amide II, sulfate, and sugar peaks from individual FTIR spectra which are 1,605-1,685 $cm^{-1}$, 1,490-1,585 $cm^{-1}$, 1,185-1,290 $cm^{-1}$, and 960-1,185 $cm^{-1}$, respectively, were integrated between the above ranges. Previous studies have reported these values for articular cartilage and were adjusted to match the peak values found in TMJ cartilage (Boskey *et al*., 1992; Boskey and Pleshko Camacho, 2007; Camacho *et al*., 2001; Khanarian *et al*., 2014; Silverberg *et al*., 2014; Sloan *et al*., 2020; Spalazzi *et al*., 2013). The area under the curve was obtained by plotting a line between the wavenumbers for each peak and integrating under the spectrum (Boskey and Pleshko Camacho, 2007; Camacho *et al*., 2001; Khanarian *et al*., 2014; Spalazzi *et al*., 2013; Kim *et al*., 2005). The values obtained from peak integration were divided into groups from the articular surface through the subchondral bone to obtain the depth-dependent normalized peak area values for all porcine, canine, and human samples. Previous studies have shown that pure type I collagen showed notable peaks in amide I, amide II, and sulfate regions. Pure aggrecan also had notable peaks in the amide I, sulfate regions and had a large peak in the sugar region while lacking a peak in the amide II region (Sloan *et al*., 2020). Therefore, the amide II peak was chosen to represent collagen, while the sugar peak was chosen to represent proteoglycans (Fig. 1**d**).

**Mechanical shear testing via TDIS/confocal microscope**

All samples were cryotomed on the subchondral bone side and rectangular surface of the hemicylinder explants to ensure a perpendicular mount and flat surface for visualization. Using a previously established protocol, (Buckley *et al*., 2010) samples were stained in 14 μg/mL 5-dicholorotriazinyl-aminofluorscein (5-DTAF) (Sigma, St. Louis, MO, USA) and imaged under an inverted Zeiss LSM 510 5 live confocal microscope (Carl Zeiss ag, Oberkochen, Germany) at 488 nm laser wavelength. The hemicylindrical explant was mounted on a custom tissue deformation imaging stage (TDIS) where 10 % global axial strain was applied. The tissue was allowed to equilibrate for 30 minutes, and five lines perpendicular to the articular surface were photobleached to track deformation of the tissue. A 3 % oscillatory shear strain was applied at 1 Hz to replicate the motion of the human jaw and live videos were recorded for further data analysis (Fig. 1**e**).

*Shear modulus data analysis*

Shear modulus was calculated using a custom MATLAB (Mathworks, Natick, MA, USA) algorithm (Buckley *et al*., 2013) which tracked the displacement of the five photobleached lines throughout the depth of the cartilage and deriving these values to get shear strain. The stress was calculated by the known force applied by calibrated springs of the TDIS plate and divided by the sample to plate contact area. Shear modulus was then obtained by dividing shear stress by shear strain as a function of depth to obtain the depth-dependent shear modulus (Fig. 1**h**).

*Gray value intensity of 5-DTAF stain*

Analysis of the confocal micrographs was performed on ImageJ (NIH, Bethesda, MD, USA) by measuring the gray value pixel intensity. A region of interest (ROI) was selected in the four regions between the five photobleached lines and the gray value pixel intensity values were averaged throughout the depth of the tissue (Fig. 1**f**).

*Fast Fourier transformation*

Analysis of the confocal micrographs was performed using Fast Fourier Transform (FFTs). ROI was selected to be 75 px × 75 px to include the area between photobleached lines and were moved from the articular surface throughout the depth of the tissue by 1 px increments. All four regions between the five photobleached lines were measured. 2D FFTs were calculated for every ROI and were binarized to have a pixel intensity of either 1 or 0. Each ROI was rotated by 10-degree increments and center two rows of pixels were averaged. The maximum average pixel intensity was calculated as a function of angle. This value was then divided by the average pixel intensity orthogonal to the angle of the maximum average

pixel intensity and was used as an orientation index (OI). The angle of rotation at which the orientation index occurred was also recorded. These values were plotted throughout the depth of the tissue and determined the orientation and direction of the orientation of the tissue (Boys *et al.*, 2019) (Fig. 1**g**).

### Statistical analysis

Pearson's correlation was used to explain the relationship between % intensity of the confocal micrographs and FTIR measurements. Linear regression was used to estimate the slope and intercept of correlation plots of composition and structure. All analysis was performed in R Studio (Posit Software, Boston, MA, USA) and MATLAB.

## Results

Histological staining revealed the zonal structures of the TMJ cartilage. As we have noted in a previous finding (Gologorsky *et al.*, 2021), porcine samples showed four distinct zones ([I]~[IV]) distinguished by collagen, proteoglycan content and cells. Zone [I] was observed to have high collagen content and no proteoglycans. Zone [II] showed less collagen content with higher cell density than Zone [I]. Increase in proteoglycans was observed as well as hypertrophic chondrocytes in Zone [III]. Zone [IV]

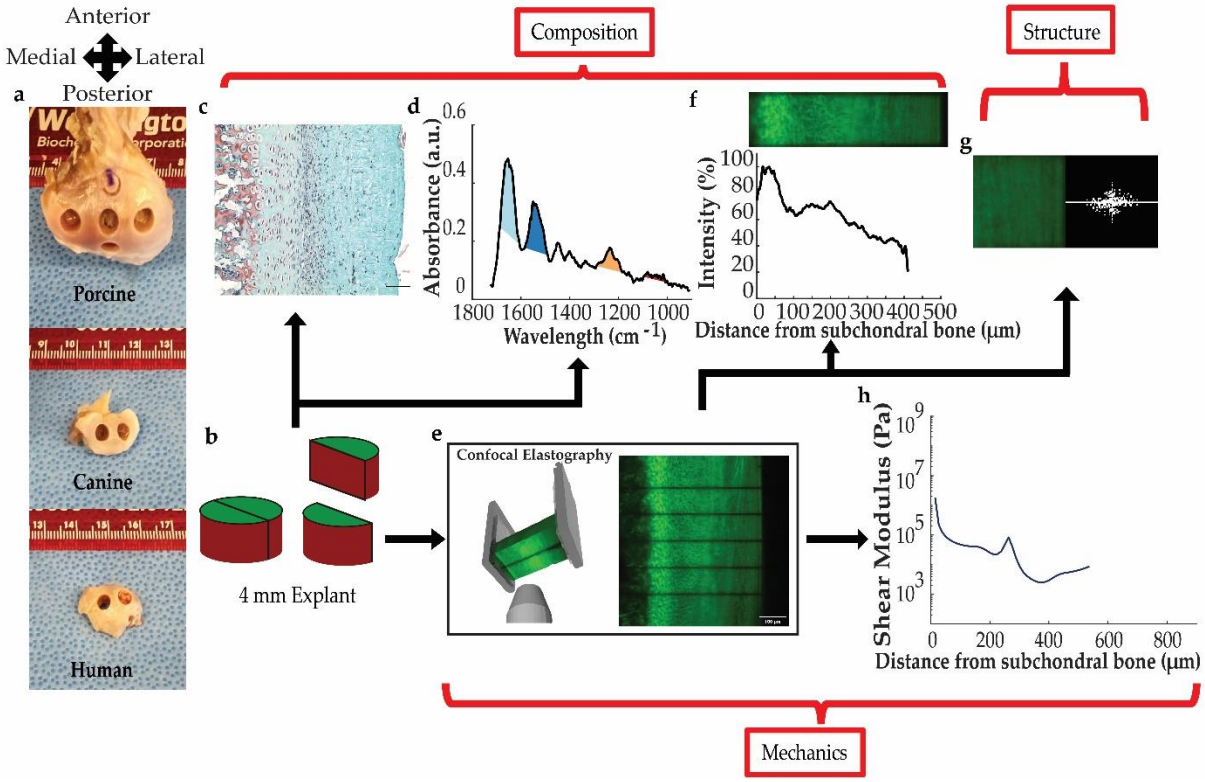


**Fig. 1. Flowchart of methods used for analyzing TMJ cartilage composition, structure, and mechanics.** (**a**) Mandibular condyles of porcine, canine, and human cadavers punched in respective anatomic locations. (**b**) 4 mm osteochondral explants bisected in the posteroanterior direction. (**c,d**) One half of the explants is used for histological staining and FTIR microscopy for compositional analysis. (**e**) One half is used for confocal elastography for mechanical testing. (**f**) Confocal micrograph is then used for gray value intensity measurements of 5-DTAF. (**g**) Confocal micrographs are analyzed with FFT for structural measurements. (**h**) Confocal micrographs are analyzed for measuring shear mechanics. TMJ, temporomandibular joint; 5-DTAF, 5-dicholorotriazinyl-aminofluorscein; FFT, Fast Fourier transformation.

had the largest cells oriented in columns with high proteoglycan content and increasing hypertrophy (Fig. 2**a**). Also, as seen in the picrosirius red stain under polarized light images (Fig. 2**b**), the surface has an abundance of highly aligned fibers that were not existent in the regions closer to the subchondral bone (Table 1). Notably, unlike porcine samples that had four distinct zones, canine and human samples showed two to three distinct zones. Canine samples lacked the surface fibrous Zone [I], while human samples lacked both the surface fibrous Zone [I] and the proliferative Zone [II]. As such, histology indicated that the three species: porcine, canine, and human, had different number of zones in the TMJ cartilage.

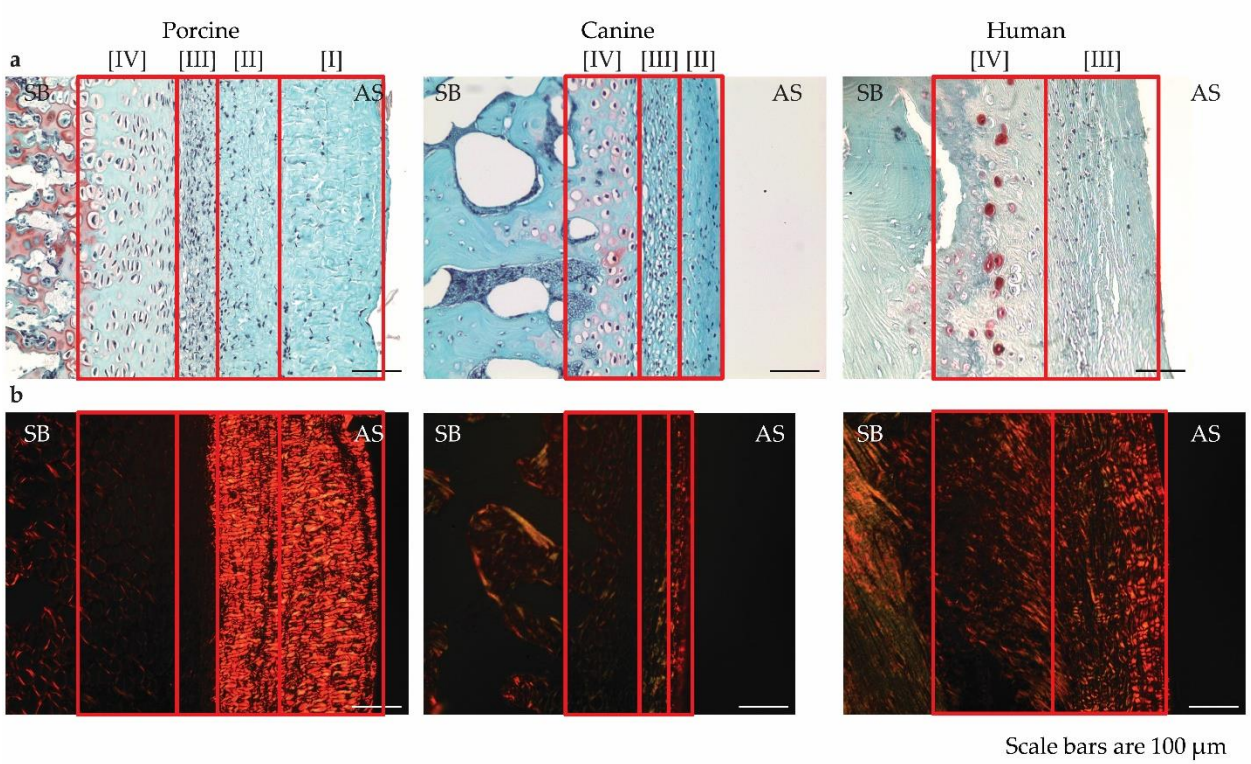


**Fig. 2. Qualitative zonal structural features ([I]~[IV]) and fiber orientation between species were seen in Safranin-O (a) and Picrosirius red stain under polarized light (b).** All scale bars are 100 μm.

**Table 1. Zonal features observed from safranin-O and picrosirius red stain observed under polarized light histology of TMJ cartilage.**

| Zone | Proteoglycan content | Collagen content | Chondrocyte characteristics |
|---|---|---|---|
| **I** | None | High | Low to no trace |
| **II** | None/Low | High/Medium | Low density and sparsely spaced |
| **III** | Low/Medium | Medium/Low | small and densely packed |
| **IV** | High | Low | Vertically streched and large |

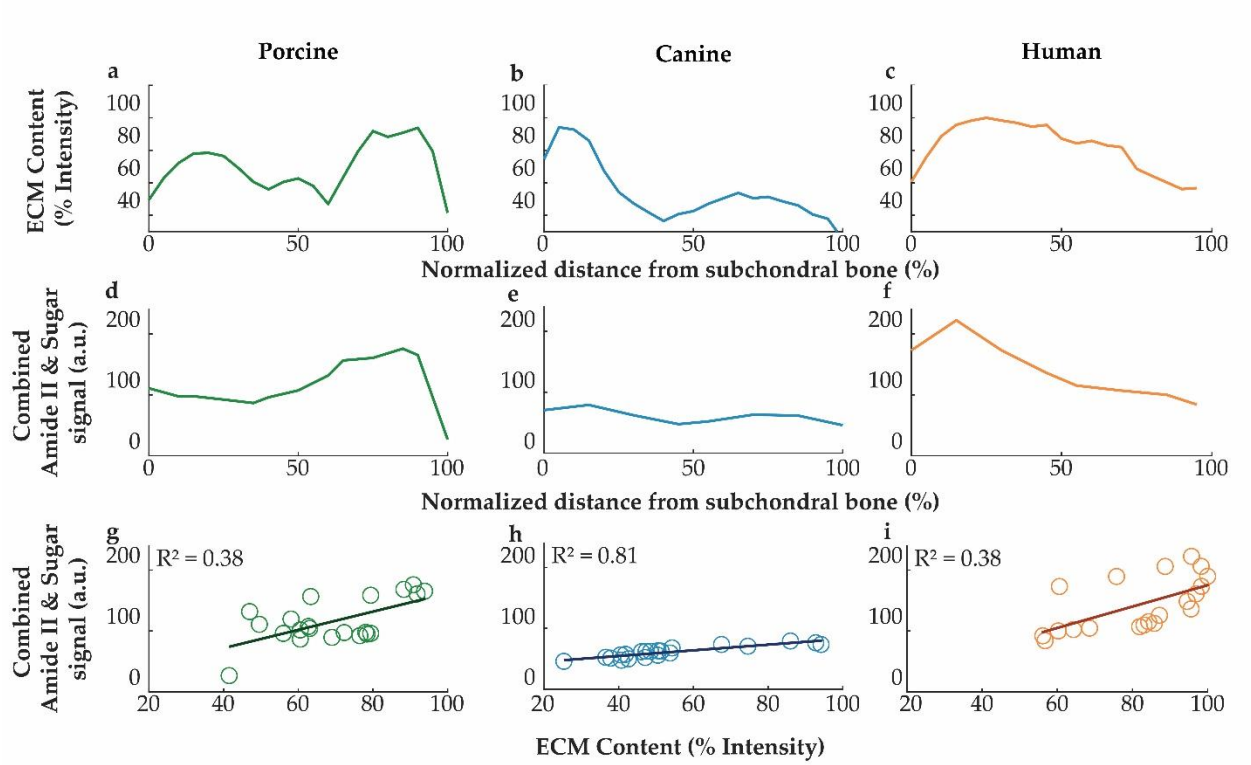


**Fig. 3. Extracellular Matrix (ECM) Content (% Intensity) (a,b,c), FTIR measurements (d,e,f), and correlation plots (g,h,i) represent 5-DTAF intensity as a measurement of relative protein content.**

Histology showed composition and structure in a qualitative manner. To quantify the compositional aspects of TMJ cartilage, we performed FTIR microscopy on unstained tissue section. To capture total extracellular matrix (ECM) density, we assessed the weighted combination of integrated absorbance (a.u.) of amide II and sugar representing collagen and proteoglycan respectively (Fig. 3**d~f**). Additionally, we used intensity of 5-DTAF staining from confocal microscopy as an assessment of total ECM content (Fig. 3**a~c**). To compare these two different techniques, the thicknesses of the samples were normalized due to the difference in testing environments. ECM content measured from the confocal micrographs were compressed by 10 % in the axial direction. However, the absorbance measured from FTIR were uncompressed samples.

Notably, ECM content measured from confocal micrographs showed a high intensity at sites closer to the subchondral bone. The porcine sample which had all four zones ([I]~[IV]) as seen from histology, showed an increase in intensity at regions near the surface. The absorbance measured from FTIR showed a similar pattern to the intensity measurements from confocal micrographs. Regions closer to the subchondral bone had higher combined amide II & sugar signal, and notably porcine samples also had a higher signal at the surface region.

To compare these distinct measurements of ECM content, correlation between confocal intensity and FTIR were performed on individual samples (Fig. 3**g~i**). The correlation between the two measurements showed a linear increase with $R^2$ values of 0.38, 0.81, and 0.38 for porcine, canine, and human samples respectively. The correlation between quantitative measurements of ECM content and FTIR absorbance yields that ECM content measured from confocal micrographs can be used as a surrogate measurement of real-time live local composition.

As we have quantified compositional measurements from FTIR and confocal micrograph analysis, quantification of the structure of TMJ cartilage was performed by using FFT analysis on confocal micrographs throughout the depth of the tissue. (Fig. 4**a**) Orientation index plotted against the normalized depth for the three species showed values higher than 1.4 in the surface regions. Regions closer to the subchondral bone gave values closer to 1 (Fig. 4**b**). The decrease in orientation index deeper into the tissue is due to the increase in random orientation of the fibers as well as the appearance of chondrocytes. For the angle of orientation, all three species measured angles close to 0° (parallel to articular surface) at regions closer to the surface. Quantitative structural analysis (Fig. 4**c**) confirmed our observation from histology where the picrosirius red stain observed under polarized light (Fig. 2**b**) had higher fiber orientation near the surface.

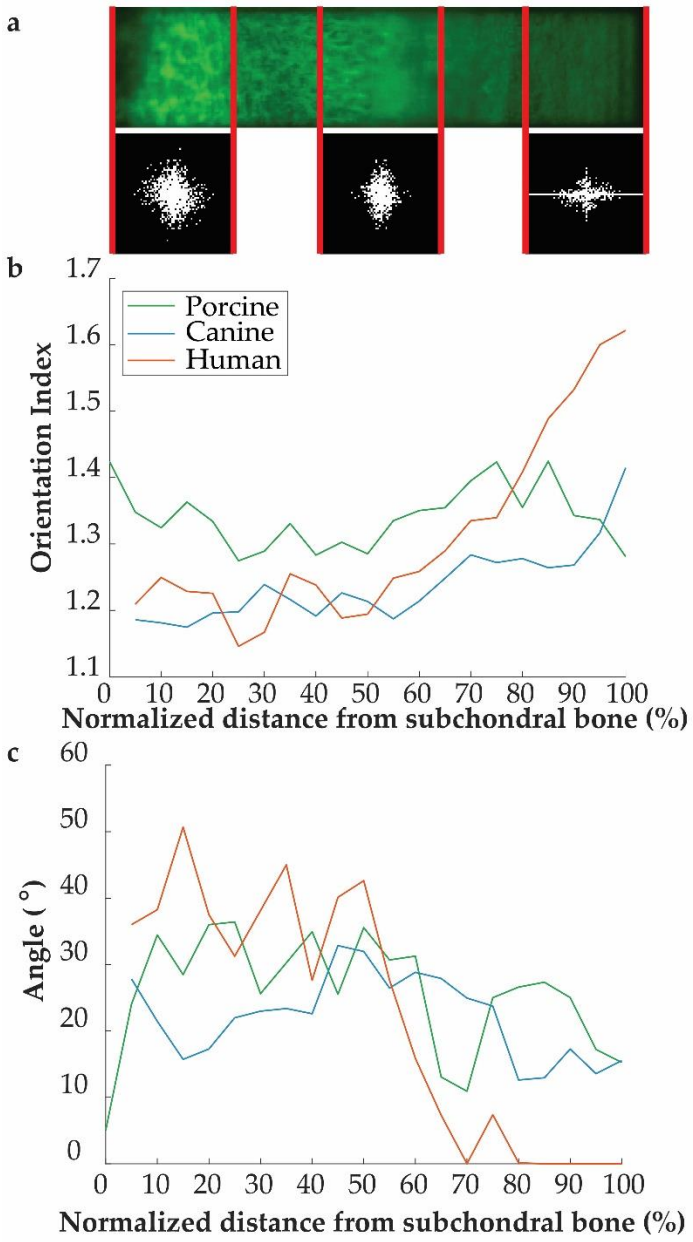


**Fig. 4. Structural analysis of confocal micrographs using FFT (a) show that the fibrous surface region has high fiber alignment (b) in the direction of shear applied (c).**

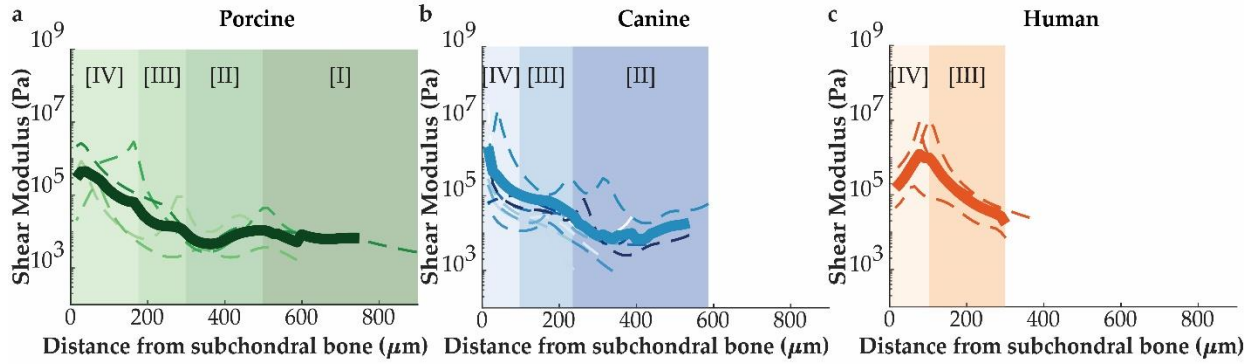


**Fig. 5. Local shear modulus plotted against the distance from the subchondral bone show distinct zonal mechanical features for porcine (a), canine (b), and human (c) cartilage.**

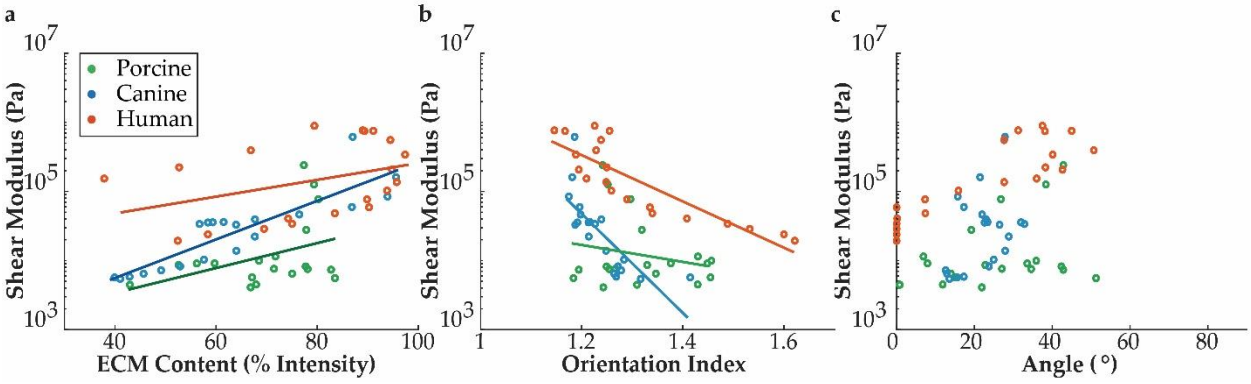


**Fig. 6. Correlation of shear modulus with composition and structure show ECM content (a) and fiber alignment (b~c) contributes to overall tissue stiffness.**

To investigate the mechanics of the TMJ cartilage, the depth-dependent shear modulus was obtained in all three species. Depth-dependent shear modulus values aligned from the subchondral bone showed distinct zonal differences. Porcine samples which exhibited the largest thickness had shear modulus profiles consistent with all four zones ([I]~[IV]) (Table 2). The hypertrophic zone (Zone IV) had the highest average shear modulus range of $10^5$~$10^7$ Pa with an average thickness of 100 μm. The mature zone (Zone III) showed a decreasing trend from the hypertrophic zone with an average shear modulus range between $10^3$~$10^5$ Pa with a thickness of 200 μm or a distance of 100~300 μm from the subchondral bone. The proliferative zone (Zone II) plateaued until 450 μm and increased slightly with an average shear modulus range of $10^3$ Pa. The fibrous surface zone (Zone I) had the lowest shear modulus range of $10^3$ Pa and was the thickest zone to be 300 μm (Fig. 5**a**). Canine samples exhibited a similar shear modulus profile as porcine samples apart from the absence of the fibrous zone (Zone I). Canine hypertrophic zone (Zone IV) had an average shear modulus range of $10^5$~$10^7$ Pa samples and followed a similar decrease with a plateau at the mature and proliferative zones similarly to porcine samples with an average shear modulus range of $10^3$~$10^4$ Pa (Fig. 5**b**). The shear modulus profile of human TMJ cartilage resembled the other

**Table 2. Total thickness measurements and thickness for zonal regions of porcine, canine, and human TMJ samples.**

| | Avg Thickness (μm) | n | [IV] (μm) | [III] (μm) | [II] (μm) | [I] (μm) |
|---|---|---|---|---|---|---|
| **Porcine** | 677 ± 156 | 4 | 239 ± 64 | 128 ± 52 | 107 ± 13 | 192 ± 35 |
| **Canine** | 374 ± 88 | 10 | 82 ± 15 | 124 ± 14 | 128 ± 35 | |
| **Human** | 321 ± 31 | 3 | 121 ± 11 | 179 ± 2 | | |

**Table 3. Correlation between shear modulus and ECM content, orientation index, and angle show statistically significant relations.** Slopes have no statistically significant differences. Signif. Codes 0 '***' 0.001 '**' 0.01 '*' 0.05 '.' 0.1 ' ' 1.

| $R^2$ | SM vs ECM Content | SM vs OI | SM vs Angle |
|---|---|---|---|
| **Porcine** | 0.15 '.' | 0.05 '*' | 0.11 ' ' |
| **Canine** | 0.77 '***' | 0.59 '***' | 0.16 '.' |
| **Human** | 0.38 '**' | 0.71 '***' | 0.70 '***' |

two species but lacked the proliferative zone and fibrous surface zones. The average shear modulus ranged from 103~105 Pa (Fig. 5**c**). Overall, all three species had similar characteristics of high shear modulus near the subchondral bone and a decrease when progressing towards the surface. However, notably, the human samples had higher overall stiffness compared to canine and porcine samples.

To quantitatively assess the relationship of how composition and structure affects the local mechanics of TMJ cartilage, ECM content, orientation index, and angle of orientation was correlated to the depth-dependent local shear mechanics (Table 3). Composition plotted against local shear mechanics on a log-linear scale showed that ECM content had a positive correlation to the local shear mechanics. This correlation showed that there are orders of magnitudes (four to fourteen-fold of the fit lines) increase in shear modulus with small changes (two-fold) of ECM content. The slope of the fit lines for the three species had no statistically significant differences except between the porcine and canine ($p < 0.05$). However, an increase in elevation of the fit lines between species was observed. Human samples exhibited average shear modulus values that were almost an order of magnitude higher than porcine samples (Fig. 6**a**).

Orientation index plotted against the shear mechanics for the canine and human tissue showed a negative correlation. The regions with highest orientation index corresponded to low shear modulus values and these regions were observed to be the fibrous surface region. Low OI regions had high shear modulus values that corresponded with the randomization of fiber orientation in the deep zones of the tissue as well as the appearance of chondrocytes (Fig. 6**b**).

Angle of orientation plotted against the shear modulus did not show any significant correlation except for the human tissue. However, the angle of orientation of the surface fibrous region was lower and mostly parallel to the shearing direction upon qualitative observation of the confocal micrographs (Fig. 6**c**). Overall, all three species showed similar trends of positive correlation for composition, and negative correlation for orientation index. However, notably human samples were stiffer than other species with respect to composition and structure.

## Discussion

The objective of this study was to compare the zonal shear mechanics of young porcine TMJ cartilage which is used in many disease and degeneration models, to tissue from canine and humans which are known to naturally develop disease. The stiffness in the hypertrophic zone was similarly high in all three species. In contrast, porcine tissue had a thicker, more compliant fibrous zone that was largely absent in canine and human tissue. Similarly, the hypertrophic zone in all three species had high proteoglycan content, while the surface regions had higher collagen content and fiber orientation. As such, the structural and compositional properties were correlated to the local shear mechanics. It was found that ECM density was highly correlated with the shear mechanics. On the other hand, orientation index was inversely correlated with shear modulus and orientation angle was poorly correlated with the shear modulus. Thus, while composition and structure underlying the local mechanics in all three species were similar, the thick, more compliant fibrous zone in porcine tissue distinguishes itself from canine and human tissue.

Histology images showed critical differences in the zonal structures of porcine, canine, and human tissues. The absence of surface zones in canine and human samples resulted in these tissues being substantially thinner than porcine samples. Qualitatively, zonal differences were characterized by the appearance, orientation, and size of chondrocytes as well as differences in proteoglycan content. Porcine samples were observed to have four zones as has been reported in previous studies (Almarza and Athanasiou, 2004; Gologorsky *et al*., 2021; Hinton and Carlson, 2005; Luder, 1998; Singh and Detamore, 2009). Canine samples were observed to be mostly missing the fibrous surface (Zone I), which in contrast to Sant'Anna *et al*. (2007), which showed a fibrous region existing. Notably, the animals used in this previous study were 6~8 months old and skeletally immature, which this current study used canines that were all over 1 year of age. Human samples were observed to be missing the fibrous surface (Zone I) and the proliferative zone (Zone II). Notably, human cadaver samples used in this study were relatively free of any severe disease or degeneration, which is scarce in literature. An interesting feature of the TMJ cartilage seen in the Safranin-O stains is that the relative proteoglycan content is lower to the overall collagen composition of the tissue and is mainly seen only near regions close to the subchondral bone. Collectively, these data point to differences in the zonal composition and structure in TMJ cartilage due to species, age, and disease state.

Quantifying ECM content in TMJ cartilage is critical to understanding the local composition of this unique and complicated joint. 5-DTAF is a general protein stain, that binds to amines and has been used widely to image cartilage for elastography (Bartell *et al*., 2015; Buckley *et al*., 2008; Buckley *et al*., 2010; Gologorsky *et al*., 2020; Silverberg *et al*., 2014; Wyse Jackson *et al*., 2022). The non-specific nature of 5-DTAF binding should yield intensities that are proportional to general protein (and hence ECM) content. However, this idea has never been tested. We found that 5-DTAF intensity was highly correlated to the weighted sum of collagen and proteoglycan content obtained by FTIR microscopy. FTIR microscopy has been widely used in measuring compositional properties in many other types of cartilage (DiDomenico *et al*., 2019; Silverberg *et al*., 2014; Sloan *et al*., 2020; Wyse Jackson *et al*., 2022). However, FTIR microscopy has not been performed to measure the local composition of TMJ cartilage to the best of our knowledge. Notably local composition from FTIR has been shown to be predictive of local mechanics of articular cartilage (DiDomenico *et al*., 2019; Middendorf *et al*., 2020; Silverberg *et al*., 2014; Wyse Jackson *et al*., 2022). Based on the correlation between 5-DTAF intensity and FTIR, we investigated whether 5-DTAF staining intensity was correlated to the local shear mechanics. This approach has the additional benefit that it yields the compositional information on tissue in the compressed state in which shear testing is performed. The ability to directly compare mechanical and structural information to the shear mechanics of the tissue can help understand the complicated function of this tissue. This technique

is not just applicable to TMJ tissue alone but may be applied to other types of tissue. Collectively, measuring ECM content from 5-DTAF stained confocal micrograph can serve as a good prediction of the highly non-linear nature of the shear mechanics. In addition to compositional analysis, structure and organization may also play an important role in dictating the local mechanics. FFT analysis measured orientation index, which showed higher magnitude of alignment of fibers in zones closer to the surface (Zone I). Notably, this region was the least stiff. As a result, OI was inversely correlated to the shear modulus. The angle of orientation showed fibers closer to the surface region were parallel to the direction of the applied mechanical shear from the confocal micrographs. This surface region, parallel to the region of high OI, is likely to experience sliding of fibers in the direction of shear, which is analogous to chewing, therefore resulting in a lower shear modulus. As we proceed closer to the subchondral bone, the tissue exhibits more randomly aligned fibers as well as shows the appearance of chondrocytes which decreases the orientation index, as well as increase the angle of the orientation further away from the parallel shearing surface. As a whole, these data show that the shear modulus of the surface region of TMJ cartilage is dictated by fiber sliding of the surface.

TMJ cartilage of all three species shared distinct mechanical properties in distinct structural zones of the tissue. These distinct zonal mechanics create high stiffness gradients of magnitudes. All three species had the highest shear modulus in the hypertrophic zone (Zone IV) which decreased with distance from the subchondral bone. Comparing the zonal mechanics is difficult in porcine, canine, and human species because the overall thickness and zonal thickness are different. Porcine samples had four, canine samples had three, and human samples had two distinct mechanical zones. The missing zones were the fibrous and proliferative zones (Zone I and Zone II), which align with the surface being the area most affected to stress and degeneration (Sindelar and Herring, 2005). While studies of depth dependent properties of the cartilage have mainly observed features from the surface (Gologorsky *et al*., 2020; Silverberg *et al*., 2014; Wyse Jackson *et al*., 2022). The lack of surface regions in canine and human TMJ cartilage samples make this approach problematic. As a result, we referenced from the subchondral bone which nicely aligns the local mechanical properties in porcine, canine, and human samples. As seen in all three species, the deep hypertrophic region (Zone IV) is preserved, and this may be due to the fact that it is not the bone that fails but it is more likely that the soft articulating surface of the tissue fails. As such, this approach may provide a consistent framework in studying healthy and diseased tissue.

Combining our analyses of composition and structure to the mechanics reveal important features. Notably, the correlation between composition and shear modulus was log-linear, indicating that small changes in collagen composition lead to magnitudes of changes in the shear modulus. The log-linear relationship gives unique insight to the function of this tissue. This non-linear relationship was similar among all three species. For example, in all three species, increasing ECM content by two-fold (40~80 %) increased the shear modulus by a factor of four to fourteen times. While the dependence on composition was similar, the elevation of these curves was different, indicating baseline stiffness of canine and human samples was higher than porcine samples.

There was also a negative correlation between OI and shear modulus. Such result indicates more aligned tissue is more compliant. This characteristic of the tissue compliance is mainly due to sliding effects in the surface. The surface of TMJ cartilage is highly aligned and is in contrast to previous findings which local fiber organization is qualitatively uncorrelated with the shear mechanics (Silverberg *et al*., 2014). This difference in behavior of TMJ cartilage to knee and ankle cartilage is likely due to the fact that the highly fibrous surface zone is absent in articular cartilage in other joints. Furthermore, the angle of orientation of the fibers is not predictive of shear modulus which aligns with previous studies of articular cartilage in the knee (Silverberg *et al*., 2014).

TMJ condylar cartilage differs from articular cartilage from other joints due to the presence of type I collagen (Wang *et al*., 2009). The fibrous superficial zone is composed of type I collagen as

well as type III collagen. Unlike hyaline cartilage, which type II collagen is the main component, type II collagen is observed mostly in the mature and hypertrophic zones in TMJ cartilage as well as type X collagen. (Delatte *et al*., 2004; Kuroda *et al*., 2009) The collagen network in articular cartilage is known to impact the form, stability, tensile strength, and resistance to shear force. Notably, the different types of collagens as well as proteoglycans in the ECM have different roles. Type I collagen is known to form thick collagen fibers (~ 60 nm) that are also regulated by type III collagen that occur mainly in the superficial zone. In the deeper mature and hypertrophic zones, type II collagen forms thinner collagen fibers (~ 30 nm) and are reinforced by proteoglycans embedded in the collagen network. The thickness and orientation of the collagen fibers formed by different collagen types, and reinforcement of proteoglycans in the different zones differentiates the resistance to shear as shown in Fig. 5. The collagen type I dominant superficial layer suggests that tension to be the primary mode of load, and compression to be the primary mode of load in the type II dominant mature and hypertrophic zones (Singh and Detamore, 2009). As such, understanding the contribution of the different collagen types to the mechanics is important. These collagen types differ not only mechanically but also in fiber size which would affect how the fibers react to bending. The importance of the contributions of fiber size, direction, and density have been brought up with relatively new theory for cartilaginous tissues called the rigidity percolation.

Recently, a new theoretical framework has been used to explain the molecular origins of articular cartilage shear mechanics (Michel *et al*., 2022; Silverberg *et al*., 2014; Wyse Jackson *et al*., 2022). Termed rigidity percolation, this framework understands the ECM as a network of bonds that represent the collagen matrix. The shear modulus of a sparsely populated network is quite low, while a dense connected network is quite stiff. Near the threshold of network connectivity, stiffness is highly sensitive to matrix density such that adding a small amount of matrix can dramatically change the shear modulus. Our data are consistent with this theory – two-fold change in matrix density resulted in a four to fourteen-fold increase in shear modulus. This non-linear relationship has been modeled to be exponential (Silverberg *et al*., 2014)

$$|G^*(V_C)| \sim (V_C - V_0)^{\xi}$$

where $G^*$ represents shear modulus, $V_C$ represents collagen volume fraction, $V_0$ represents threshold volume fraction, and $\xi$ represents the exponent of the fit which was $4.5 \pm 0.1$. Notably, the exponent observed here for this study

$$|G^*(I)| \sim (I)^{\xi}$$

where $I$ represents ECM content (% Intensity) was more compliant ($\xi = 1.96 \pm 0.27$) than to that of reported for articular cartilage (Silverberg *et al*., 2014). Interestingly, porcine data which includes a larger portion of highly aligned surface region has lower shear modulus than canine and human samples. Recent studies of more highly aligned networks show perturbations to the percolation threshold that may explain the more compliant nature of porcine TMJ cartilage (Michel *et al*., 2022). Further work is needed to directly apply rigidity percolation theory to TMJ cartilage.

Another potential explanation for the difference in elevation of stiffness are levels of collagen crosslinking. ECM changes prominently by collagen crosslinking during aging (Aït-Belkacem *et al*., 2012; Bai *et al*., 1992; Brüel and Oxland, 1996; Tang *et al*., 2007). Furthermore, increase in stiffness has been documented by collagen crosslinking that naturally occurs by aging (Chen *et al*., 2020; Handl *et al*., 2007; Mirahmadi *et al*., 2018). Porcine samples used in this study were young while canine and human samples were considered mature. As such, the difference in stiffness may be caused by difference in levels of collagen crosslinking due to age.

This study shows that pigs normally used have a surface region of approximately 150~300 μm that is compliant. Pigs may give a good approximation for properties of the surface region however, this surface region is not present in adult canine and humans. As such, histological, biological, and mechanical studies of TMJ cartilage should focus on the deep regions closer to the subchondral bone that exist in species that can develop naturally occurring disease such as canine and human. There is still much to reveal about the properties of TMJ cartilage. This study investigated the relationship

between microscale shear modulus, composition, and structure in porcine, canine, and human TMJ cartilage and therefore help understand the complex function of this joint.

## Conclusions

This study combined state of the art techniques to investigate the microscale compositional, structural, and mechanical properties of the TMJ condylar cartilage in porcine, canine, and human tissue. All three species had distinct mechanical properties that varied by structural zones yielding high gradients in modulus (*e.g.* 100-fold change over 250 μm). These modulus gradients arose from gradients in composition. The relationship between composition and mechanics was highly non-linear, with a two-fold increase in matrix density leading to a twenty-fold increase in shear modulus. This non-linearity is consistent with a rigidity-percolation threshold in the tissue that governs local mechanics. Notably more highly oriented regions of the tissue were more compliant, suggesting that fiber sliding dominates the shear mechanics of the surface zone. Furthermore, angle of fiber orientation was not predictive of shear mechanics. While these relationships were true for all three species investigated, the skeletally immature pig TMJ, frequently used for disease models has a thick surface absent in canine and human tissue. Presence of this surface zone is likely to affect the degeneration process in TMJ cartilage and as such must be taken into account when interpreting disease, degeneration, as well as regeneration.

## Acknowledgements

We thank Cornell Center for Materials Research (CCMR), Cohen lab members, and the Schaffer-Nishimura lab for their assistance in training for FTIR microscopy, TDIS confocal elastography, and cryotome.

## Author contributions

Conception: All authors; study design: D.Y., I.C., L.J.B.; performed experiments: D.Y.; critical interpretation of results: D.Y., I.C., L.J.B.; drafted the manuscript: D.Y., L.J.B.; read and edited the manuscript: all authors.

## Ethics approval and consent to participate

All of the tissues used for these studies are from cadaveric sources. Cornell considers obtaining cadaveric tissue to be exempt from IACUC (animal) and IRB (human) approval.

## Funding

This work was funded by the National Science Foundation under grant CMMI – 1927197.

## Conflict of interest

Dr. Bonassar is a co-founder of and holds equity in 3DBio Corp.

## References

Aït-Belkacem D (2012) Microscopic structural study of collagen aging in isolated fibrils using polarized second harmonic generation. J Biomed Opt **17**: 080506-1. DOI: 10.1117/1.JBO.17.8.080506.

Almarza AJ, Brown BN, Arzi B, Ângelo DF, Chung W, Badylak SF, Detamore M (2018) Preclinical Animal Models for Temporomandibular Joint Tissue Engineering. Tissue Eng Part B Rev **24**: 171-178. DOI: 10.1089/ten.teb.2017.0341.

Alomar X, Medrano J, Cabratosa J, Clavero JA, Lorente M, Serra I, Monill JM, Salvador A (2007) Anatomy of the temporomandibular joint. Semin Ultrasound CT MR **28**: 170-183. DOI: 10.1053/j.sult.2007.02.002.

Arzi B, Vapniarsky N, Fulton A, Verstraete FJM (2021) Management of Septic Arthritis of the Temporomandibular Joint in Dogs. Front Vet Sci **8**: 648766. DOI: 10.3389/fvets.2021.648766.

Bai P, Phua K, Hardt T, Cernadas M, Brodsky B (1992) Glycation alters collagen fibril organization. Connect Tissue Res **28**: 1-12. DOI: 10.3109/03008209209014224.

Bartell LR, Fortier LA, Bonassar LJ, Cohen I (2015) Measuring microscale strain fields in articular cartilage during rapid impact reveals thresholds for chondrocyte death and a protective role for the superficial layer. J Biomech **48**: 3440-3446. DOI: 10.1016/j.jbiomech.2015.05.035.

Boskey AL, Pleshko N, Doty SB, Mendelsohn R (1992) Applications of Fourier Transform Infrared (FT-IR) Microscopy to the Study of Mineralization in Bone and Cartilage. Cells Mater **2**: 4.

Boskey A, Pleshko Camacho N (2007) FT-IR imaging of native and tissue-engineered bone and cartilage. Biomaterials **28**: 2465-2478. DOI: 10.1016/j.biomaterials.2006.11.043.

Boys AJ, Kunitake JAMR, Henak CR, Cohen I, Estroff LA, Bonassar LJ (2019) Understanding the Stiff-to-Compliant Transition of the Meniscal Attachments by Spatial Correlation of Composition, Structure, and Mechanics. ACS Appl Mater Interfaces **11**: 26559-26570. DOI: 10.1021/acsami.9b03595.

Brüel A, Oxlund H (1996) Changes in biomechanical properties, composition of collagen and elastin, and advanced glycation endproducts of the rat aorta in relation to age. Atherosclerosis **127**: 155-165. DOI: 10.1016/s0021-9150(96)05947-3.

Buckley MR, Bergou AJ, Fouchard J, Bonassar LJ, Cohen I (2010) High-resolution spatial mapping of shear properties in cartilage. J Biomech **43**: 796-800. DOI: 10.1016/j.jbiomech.2009.10.012.

Buckley MR, Bonassar LJ, Cohen I (2013) Localization of Viscous Behavior and Shear Energy Dissipation in Articular Cartilage Under Dynamic Shear Loading. J Biomech Eng **135**: 31002. DOI: 10.1115/1.4007454.

Buckley MR, Gleghorn JP, Bonassar LJ, Cohen I (2008) Mapping the depth dependence of shear properties in articular cartilage. J Biomech **41**: 2430-2437. DOI: 10.1016/j.jbiomech.2008.05.021.

Camacho NP, West P, Torzilli PA, Mendelsohn R (2001) FTIR microscopic imaging of collagen and proteoglycan in bovine cartilage. Biopolymers **62**: 1-8. DOI: 10.1002/1097-0282(2001)62:1<1::AID-BIP10>3.0.CO;2-O.

Chen PJ, Dutra EH, Mehta S, O'Brien MH, Yadav S (2020) Age-related changes in the cartilage of the temporomandibular joint. Geroscience **42**: 995-1004. DOI: 10.1007/s11357-020-00160-w.

Costen JB (1997) A syndrome of ear and sinus symptoms dependent upon disturbed function of the temporomandibular joint. 1934. Ann Otol Rhinol Laryngol **106**: 805-819. DOI: 10.1177/000348949710601002.

Delatte M, Von den Hoff JW, van Rheden REM, Kuijpers-Jagtman AM (2004) Primary and secondary cartilages of the neonatal rat: the femoral head and the mandibular condyle. Eur J Oral Sci **112**: 156-162. DOI: 10.1111/j.0909-8836.2004.00108.x.

Detamore MS, Athanasiou KA (2003a) Structure and function of the temporomandibular joint disc: Implications for tissue engineering. J Oral Maxillofac Surg **61**: 494-506. DOI: 10.1053/joms.2003.50096.

Detamore MS, Athanasiou KA (2003b) Tensile Properties of the Porcine Temporomandibular Joint Disc. J Biomech Eng **125**: 558-565. DOI: 10.1115/1.1589778.

DiDomenico CD, Kaghazchi A, Bonassar LJ (2019) Measurement of local diffusion and composition in degraded articular cartilage reveals the unique role of surface structure in controlling macromolecular transport. J Biomech **82**: 38-45. DOI: 10.1016/j.jbiomech.2018.10.019.

Elhamian SMM, Alizadeh M, Shokrieh MM, Karimi A (2015) A depth dependent transversely isotropic micromechanic model of articular cartilage. J Mater Sci Mater Med **26**: 111. DOI: 10.1007/s10856-015-5449-8.

Gologorsky CJ, Middendorf JM, Cohen I, Bonassar LJ (2021) Depth-dependent patterns in shear modulus of temporomandibular joint cartilage correspond to tissue structure and anatomic location. J Biomech **129**: 110815. DOI: 10.1016/j.jbiomech.2021.110815.

Grant PG (1973) Biomechanical significance of the instantaneous center of rotation: The human temporomandibular joint. J Biomech **6**: 109-113. DOI: 10.1016/0021-9290(73)90080-8.

Gysi A (1921) Studies on the leverage problem of the mandible. Dent Digest **27**: 74-84, 184-190, 203-208.

Hammond G, King A, LaPaglia J (2012) Assessment of Five Oblique Radiographic Projections of the Canine Temporomandibular Joint. Vet Radiol Ultrasound **53**: 501-506. DOI: 10.1111/j.1740-8261.2012.01956.x.

Handl M, Filová E, Kubala M, Lánský Z, Koláčná L, Vorlíček J, Trč T, Amler E (2007) Fluorescent advanced glycation end products in the detection of factual stages of cartilage degeneration.

Physiol Res **56**: 235-242. DOI: 10.33549/physiolres.930934.

Hinton RJ, Carlson DS (2005) Regulation of Growth in Mandibular Condylar Cartilage. Semin Orthod **11**: 209-218. DOI: 10.1053/j.sodo.2005.07.005.

Ingawalé S, Goswami T (2009) Temporomandibular Joint: Disorders, Treatments, and Biomechanics. Ann Biomed Eng **37**: 976-996. DOI: 10.1007/s10439-009-9659-4.

Khanarian NT, Boushell MK, Spalazzi JP, Pleshko N, Boskey AL, Lu HH (2014) FTIR-I compositional mapping of the cartilage-to-bone interface as a function of tissue region and age. J Bone Miner Res **29**: 2643-2652. DOI: 10.1002/jbmr.2284.

Kim KW, Wong ME, Helfrick JF, Thomas JB, Athanasiou KA (2003) Biomechanical Tissue Characterization of the Superior Joint Space of the Porcine Temporomandibular Joint. Ann Biomed Eng **31**: 924-930. DOI: 10.1114/1.1591190.

Kim M, Bi X, Horton WE, Spencer RG, Camacho NP (2005) Fourier transform infrared imaging spectroscopic analysis of tissue engineered cartilage: histologic and biochemical correlations. J Biomed Opt **10**: 031105. DOI: 10.1117/1.1922329.

Kuboki T, Shinoda M, Orsini MG, Yamashita A (1997) Viscoelastic Properties of the Pig Temporomandibular Joint Articular Soft Tissues of the Condyle and Disc. J Dent Res **76**: 1760-1769. DOI: 10.1177/00220345970760110701.

Kuroda S, Tanimoto K, Izawa T, Fujihara S, Koolstra JH, Tanaka E (2009) Biomechanical and biochemical characteristics of the mandibular condylar cartilage. Osteoarthritis Cartilage **17**: 1408-1415. DOI: 10.1016/j.joca.2009.04.025.

Labus KM, Kuiper JP, Rawlinson J, Puttlitz CM (2021) Mechanical characterization and viscoelastic model of the ovine temporomandibular joint Disc in indentation, uniaxial tension, and biaxial tension. J Mech Behav Biomed Mater **116**: 104300. DOI: 10.1016/j.jmbbm.2020.104300.

Lowe J, Bansal R, Badylak SF, Brown BN, Chung WL, Almarza AJ (2018) Properties of the Temporomandibular Joint in Growing Pigs. J Biomech Eng **140**: 071002. DOI: 10.1115/1.4039624.

Maas CPHJ, Theyse LFH (2007) Temporomandibular joint ankylosis in cats and dogs: A report of 10 cases. Vet Comp Orthop Traumatol **20**: 192-197. DOI: 10.1160/VCOT-06-08-0062.

Macready DM, Hecht S, Craig LE, Conklin GA (2010) Magnetic Resonance Imaging Features of the Temporomandibular Joint in Normal Dogs. Vet Radiol Ultrasound **51**: 436-440. DOI: 10.1111/j.1740-8261.2010.01680.x.

Michel J, von Kessel G, Jackson TW, Bonassar LJ, Cohen I, Das M (2022) Reentrant rigidity percolation in structurally correlated filamentous networks. Phys Rev Research **4**: 043152. DOI: 10.1103/PhysRevResearch.4.043152.

Middendorf JM, Dugopolski C, Kennedy S, Blahut E, Cohen I, Bonassar LJ (2020) Heterogeneous matrix deposition in human tissue engineered cartilage changes the local shear modulus and resistance to local construct buckling. J Biomech **105**: 109760. DOI: 10.1016/j.jbiomech.2020.109760.

Milam SB (2003) Pathophysiology and epidemiology of TMJ. J Musculoskelet Neuronal Interact **3**: 382-390; discussion 406-407.

Mirahmadi F, Koolstra JH, Lobbezoo F, van Lenthe GH, Ghazanfari S, Snabel J, Stoop R, Everts V (2018) Mechanical stiffness of TMJ condylar cartilage increases after artificial aging by ribose. Arch Oral Biol **87**: 102-109. DOI: 10.1016/j.archoralbio.2017.12.010.

Piette E (1993) Anatomy of the human temporomandibular joint. An updated comprehensive review. Acta Stomatol Belg **90**: 103-127.

Sant'Anna EF, Gomez DF, Polley JW, Sumner RD, Williams JM, Figueroa AA, Bolognese AM (2007) Histological Evaluation of the Temporomandibular Joint After Bilateral Vertical Ramus Mandibular Distraction in a Canine Model. J Craniofac Surg **18**: 155-162. DOI: 10.1097/01.scs.0000248653.07663.fd.

Sharma S, Pal U, Gupta D, Jurel S (2011) Etiological factors of temporomandibular joint disorders. Natl J Maxillofac Surg **2**: 116. DOI: 10.4103/0975-5950.94463.

Silverberg JL, Barrett AR, Das M, Petersen PB, Bonassar LJ, Cohen I (2014) Structure-function relations and rigidity percolation in the shear

properties of articular cartilage. Biophys J **107**: 1721-1730. DOI: 10.1016/j.bpj.2014.08.011.

Sindelar BJ, Herring SW (2005) Soft Tissue Mechanics of the Temporomandibular Joint. Cells Tissues Organs **180**: 36-43. DOI: 10.1159/000086197.

Singh M, Detamore MS (2008) Tensile properties of the mandibular condylar cartilage. J Biomech Eng **130**: 011009. DOI: 10.1115/1.2838062.

Singh M, Detamore MS (2009) Biomechanical properties of the mandibular condylar cartilage and their relevance to the TMJ disc. J Biomech **42**: 405-417. DOI: 10.1016/j.jbiomech.2008.12.012.

Sloan SR, Wipplinger C, Kirnaz S, Delgado R, Huang S, Shvets G, Härtl R, Bonassar LJ (2020) Imaging the local biochemical content of native and injured intervertebral disc using Fourier transform infrared microscopy. JOR Spine **3**: e1121. DOI: 10.1002/jsp2.1121.

Spalazzi JP, Boskey AL, Pleshko N, Lu HH (2013) Quantitative Mapping of Matrix Content and Distribution across the Ligament-to-Bone Insertion. PLoS One **8**: e74349. DOI: 10.1371/journal.pone.0074349.

Stegenga B, de Bont LGM, van der Kuijl B, Boering G (1992) Classification of Temporomandibular Joint Osteoarthrosis and Internal Derangement. Part I: Diagnostic Significance of Clinical and Radiographic Symptoms and Signs. Cranio **10**: 96-106; discussion 116-117. DOI: 10.1080/08869634.1992.11677897.

Tanaka E, Koolstra JH (2008) Biomechanics of the Temporomandibular Joint. J Dent Res **87**: 989-991. DOI: 10.1177/154405910808701101.

Tanaka E, Yamano E, Dalla-Bona DA, Watanabe M, Inubushi T, Shirakura M, Sano R, Takahashi K, van Eijden T, Tanne K (2006) Dynamic Compressive Properties of the Mandibular Condylar Cartilage. J Dent Res **85**: 571-575. DOI: 10.1177/154405910608500618.

Tang SY, Zeenath U, Vashishth D (2007) Effects of non-enzymatic glycation on cancellous bone fragility. Bone **40**: 1144-1151. DOI: 10.1016/j.bone.2006.12.056.

Wadhwa S, Kapila S (2008) TMJ Disorders: Future Innovations in Diagnostics and Therapeutics. J Dent Educ **72**: 930-947. DOI: 10.1002/j.0022-0337.2008.72.8.tb04569.x.

Wang L, Lazebnik M, Detamore MS (2009) Hyaline cartilage cells outperform mandibular condylar cartilage cells in a TMJ fibrocartilage tissue engineering application. Osteoarthritis Cartilage **17**: 346-353. DOI: 10.1016/j.joca.2008.07.004.

Wyse Jackson T, Michel J, Lwin P, Fortier LA, Das M, Bonassar LJ, Cohen I (2022) Structural origins of cartilage shear mechanics. Sci Adv **8**: eabk2805. DOI: 10.1126/sciadv.abk2805.

**Editor's note**: The Scientific Editor responsible for this paper was Prof. Thimios Mitsiadis.